HHS Public Access

Author manuscript

*Biomaterials*. Author manuscript; available in PMC 2015 November 25.

Published in final edited form as:

*Biomaterials*. 2015 June ; 54: 63–71. doi:10.1016/j.biomaterials.2015.03.019.

# Stiffening and unfolding of early deposited-fibronectin increase proangiogenic factor secretion by breast cancer-associated stromal cells

**Karin Wang**[a,b,1], **Roberto C. Andresen Eguiluz**[a,1], **Fei Wu**[a], **Bo Ri Seo**[b], **Claudia Fischbach**[b,c], and **Delphine Gourdon**[a,b,*]

[a]Department of Materials Science and Engineering, Cornell University, Ithaca, NY 14853, USA

[b]Department of Biomedical Engineering, Cornell University, Ithaca, NY 14853, USA

[c]Kavli Institute at Cornell for Nanoscale Science, Cornell University, Ithaca, NY 14853, USA

## Abstract

Fibronectin (Fn) forms a fibrillar network that controls cell behavior in both physiological and diseased conditions including cancer. Indeed, breast cancer-associated stromal cells not only increase the quantity of deposited Fn but also modify its conformation. However, (i) the interplay between mechanical and conformational properties of early tumor-associated Fn networks and (ii) its effect on tumor vascularization remain unclear. Here, we first used the Surface Forces Apparatus to reveal that 3T3-L1 preadipocytes exposed to tumor-secreted factors generate a stiffer Fn matrix relative to control cells. We then show that this early matrix stiffening correlates with increased molecular unfolding in Fn fibers, as determined by Förster Resonance Energy Transfer. Finally, we assessed the resulting changes in adhesion and proangiogenic factor (VEGF) secretion of newly seeded 3T3-L1s, and we examined altered integrin specificity as a potential mechanism of modified cell–matrix interactions through integrin blockers. Our data indicate that tumor-conditioned Fn decreases adhesion while enhancing VEGF secretion by preadipocytes, and that an integrin switch is responsible for such changes. Collectively, our findings suggest that simultaneous stiffening and unfolding of initially deposited tumor-conditioned Fn alters both adhesion and proangiogenic behavior of surrounding stromal cells, likely promoting vascularization and growth of the breast tumor. This work enhances our knowledge of cell – Fn matrix interactions that may be exploited for other biomaterials-based applications, including advanced tissue engineering approaches.



*Corresponding author. Department of Materials Science and Engineering, Cornell University, 327 Bard Hall, Ithaca, NY 14853, USA. Tel.: +1 607 255 1623; fax: +1 607 255 2365. dg434@cornell.edu (D. Gourdon).

[1]Contributed equally.

**Author contributions**

K.W., R.C.A.E., C.F. and D.G. designed research; K.W., R.C.A.E., and F.W. performed research; K.W., R.C.A.E., F.W. and B.R.S. contributed new reagents/analytic tools; K.W., R.C.A.E. and D.G. analyzed data; and K.W., R.C.A.E., C.F., and D.G. wrote the paper.

**Appendix A. Supplementary data**

Supplementary data related to this article can be found at http://dx.doi.org/10.1016/j.biomaterials.2015.03.019.

**Keywords**

Tumor-conditioned fibronectin; Matrix stiffness; Molecular unfolding; Proangiogenic factor secretion; Integrin switch

## 1. Introduction

Varied physicochemical properties of the extracellular matrix (ECM), a dynamic and complex fibrillar network, modulate cellular behavior. In tumors, the ECM is primarily generated by cancer-associated cells (e.g. fibroblasts and adipogenic precursors) and contributes to sustained tumor growth and survival [1–8]. It exhibits numerous altered materials properties relative to normal ECM including variations in protein composition, structure, and rigidity. In fact, analysis of tumorous ECMs revealed differences in collagen I deposition relative to normal ECMs as suggested by elevated quantities, reorganization, crosslinking, and stiffness of collagen [4,9–13]. Moreover, fibronectin (Fn) might be responsible for additional ECM structural alterations, as indicated by the presence of highly stretched and unfolded Fn fibers in tumor-associated matrices [14,15]. It is important to recognize that tumor-associated Fn and collagen alterations are functionally linked since Fn (i) is essential for the deposition of collagen I in ECMs [4,16–18] and (ii) is also used as an indicator for increased tumor aggressiveness [19]. Nevertheless, a clear correlation between structural, conformational, and mechanical properties of the tumorous ECM network and the role of Fn in this process has not been established. This correlation has been hindered partly by the intrinsic complex composition of the ECM, and by the lack of analytical tools that permit simultaneous assessment of ECM materials properties from the matrix/cellular to the molecular scale. Indeed, both collagen and Fn fibers are present in mature ECM and likely synergize to modulate the bulk properties of the tumor ECM [17,20]. Additionally, there is a lack of materials science tools to separately assess morphology and mechanics of native (uncrosslinked) ECM at both matrix/cellular and molecular scales under physiologically relevant conditions.

Altered materials properties of the tumor ECM are clinically relevant as they promote tumor malignancy via direct effects on tumor cells [8] and indirectly by enhancing the formation of new blood vessels (angiogenesis) [4,9–13]. In fact, altered ECM can enhance angiogenesis either by increasing the activity of surrounding endothelial cells [14,15] or by stimulating the secretion of proangiogenic factors (e.g. vascular endothelial growth factor [VEGF]) from cancer-associated fibroblasts [4,16–18]. However, the specific ECM properties and associated mechanisms responsible for the proangiogenic capability of tumor-associated cells remain unclear.

Here, we integrated a set of physical sciences tools with cancer biology to: (i) characterize the mechanics, conformation, and topology of tumor-associated Fn matrices at both the matrix and molecular scales, and (ii) correlate these materials properties with adhesion and proangiogenic factor (VEGF) secretion of adipose stromal cells. Our results revealed that tumor-conditioned Fn matrices were stiffer and more unfolded than control matrices, and that these dysregulated matrices contributed to enhanced VEGF secretion by stromal cells.

## 2. Materials and methods

### 2.1. Cell culture

As an *in vitro* model of cancer-associated stromal cells, we utilized tumor-associated 3T3-L1 preadipocytes (ATCC, VA). Tumor soluble factors (TSF) from an aggressive metastatic breast cancer line, MDA-MB231 cells (ATCC, VA), were collected to mimic paracrine signaling between a tumor and its surrounding microenvironment. After exposing 3T3-L1s to TSF for 3 days, the preconditioned cells were detached and cultured on mica substrates for 24 h. Afterwards, culture systems were decellularized [19,21] and the resulting cell-free matrices were used for parallel mechanical, topological, and conformational characterization.

### 2.2. Surface forces apparatus

The Surface Forces Apparatus (SFA) (SurForce LLC, CA) is an interferometry-based technique that uses fringes of equal chromatic order (FECO) to quantify the absolute surface separation between two reflecting surfaces, with nm resolution, while both normal (adhesion) and lateral (friction) forces can be measured. This technique is extensively described in Refs. [17,20,22,23]. Briefly, in our study, the lower surface was mounted on a double cantilever spring of known elastic constant while the upper surface was connected to a step motor to apply normal load on the lower surface. A white light source was directed through two SFA surfaces (silica discs) previously glued with semi-reflective silvered mica, building an optical interferometer. The resulting interference FECO were directed towards the entrance slit of a photo-spectrometer (Princeton Instruments, NJ) and recorded with a CCD camera (Princeton Instruments, NJ) for further FECO analysis. The acquisition software used was LightField v4.0 (Princeton Instruments, NJ).

### 2.3. Substrate preparation for SFA characterization

Muscovite mica (S&J Trading, Australia) is a negatively charged, hydrophilic aluminosilicate that is used as preliminary substrate in all SFA experiments. To obtain transparent, uniform, and atomically smooth mica surfaces, we cleaved mica into 1 $cm^2$ sections of 2–5 μmin thickness and metallized them with 55 nm of silver to make them semi-reflective. The mica sections (silver side facing down) were then glued with UV curing glue ($E$ = 1.034 GPa, product 61) (Norland, NJ) onto semi-cylindrical silica discs of 10 mm in diameter and 20 mm of curvature radius (ESCO Products, NJ). All preparation steps were performed in a laminar flow cabinet to minimize particulate contamination. Each SFA experiment requires a pair of discs glued with mica sections cut from the same sheet to ensure equal mica thicknesses on both upper and lower discs. Customized PDMS chambers containing cell culture media were used to house the lower discs during the 24 h matrix deposition process while the upper discs (bare mica), used as indenters during force measurements, were kept clean and stored in a desiccator until needed.

### 2.4. Force curve acquisition and elastic measurements via SFA

Upper and lower SFA cylindrical discs were mounted in a crossed axis configuration to ensure a well-defined circular contact junction. The lower disc holding the ECM was

mounted on a 980 N/m spring and the upper disc (bare mica) was used to indent ECM, as depicted in Fig. 1A. The SFA stainless steel chamber was filled with 75 mL of warm (37 °C) PBS to keep the ECM in physiological conditions during mechanical characterization, and the entire system was allowed to equilibrate at 37 °C for 1 h. Each ECM was then probed at 4 different locations (approximately 500 μm apart) and each location was indented 3 consecutive times. The system was allowed to equilibrate for 30 min between each indentation and 15 min between locations. Approach (In) and retraction (Out) measurements (force runs) were performed in quasi-static conditions (at a constant speed of 0.5 μm/min) to minimize viscous effects. During force runs, FECO were acquired at a rate of 3 frames per second and post-processed with Matlab R2012b (MathWorks, MA) to yield force–distance profiles. These profiles were further analyzed to extract the compressive elastic moduli using Hertzian contact mechanics between a sphere and an elastic half-space proposed by Johnson [8,24], equation (1) (see Results).

### 2.5. Creep testing via SFA

Samples were prepared and mounted in the SFA as described in the previous section. However, the lower surface was mounted onto a more compliant spring (k = 676 N/m) and the ECM samples were indented instantaneously (rather than quasi-statically) by applying increasing step-loads of approximately 3.7 mN (indentation approximately 5 μm) using the SFA fine micrometer, resulting in forces that correspond to $F_1 = F_1' = 3.7\text{mN}, F_2 = F_2' = 7.4\text{mN}$, and $F_3' = 11.1\text{mN}$. Changes in ECM indentation depth (creep) were then monitored over 1800 s by following the shift of the FECO fringes.

### 2.6. FRET labeling of fibronectin

Alexa Fluor 488 succinimydyl ester (donor fluorophores) and Alexa Fluor 546 maleimide (acceptor fluorophores) (Invitrogen, CA) were used to label Fn for intramolecular Förster Resonance Energy Transfer (FRET) as previously described by Baneyx et al. [25] and Smith et al. [26]. Fn concentrations and labeling ratios between donors and acceptors were determined using a DU®730 UV–Vis spectrophotometer (Beckman, IN) at 280 nm, 495 nm, and 556 nm. FRET calibration of labeled Fn was first carried out in denaturant solution by varying guanidine hydrochloride concentrations between 0 and 4 M to obtain acceptor/donor intensity ratios ($I_A/I_D$), termed FRET ratios, as a function of protein denaturation. Additional FRET calibration of Fn embedded in fibers was performed via a custom-made strain device and used to correlate Fn fiber FRET ratios with fiber uniaxial strain, as described in Refs. [27,28].

### 2.7. Cell seeding and sample decellularization

3T3-L1 (ATCC, VA) preadipocytes (passages 4–10) were preconditioned for 3 days in either α-MEM culture medium (Control) or α-MEM medium containing normalized TSF. After this preconditioning period, cells were trypsinized and used for parallel SFA and FRET experiments.

Both flat mica sections (culture area: 64–81 $mm^2$/well) and curved mica surfaces (mounted on SFA discs, culture area: 80 $mm^2$/disc) in PDMS chambers were first incubated with human plasma Fn (Life Technologies, NY) at a concentration of 30 μg/mL in phosphate

buffered saline (PBS) for 60 min at room temperature to facilitate cell adhesion. After rinsing 3 times with PBS, a concentrated cell solution comprised $2 \times 10^4$ preconditioned 3T3-L1s (Control or Tumor) was seeded on the mica substrates. After 20 min of cell adhesion, 400 μL of exogenous Fn (50 μg/mL) low serum (1% fetal bovine serum (FBS)) was added. For FRET experiments, the exogenous Fn consisted of 90% unlabeled Fn (unFN) and 10% FRET-labeled Fn to prevent intermolecular FRET. For SFA experiments, only unFN was used.

After culturing at 37 °C and 5% $CO_2$ for 24 h, cultures were decellularized via a modified Cukierman protocol [21] that included deoxycholic acid incubation and extra wash steps, and left unfixed in PBS. Further samples were fixed for 1 h at 4 °C, and washed three times with PBS for immunostaining and morphology studies.

### 2.8. FRET data acquisition

Samples were imaged with a Zeiss 710 confocal microscope (Zeiss, Munich, Germany) using the C-apochromat water-immersion 40×/1.2 objective, a pinhole of 2 AU, a 488 nm laser set at 10% power, and a pixel dwell time of 6.3 μs to acquire 16-bit z-stack images spaced 2 μm apart. FRET-Fn fluorescence was simultaneously collected for the donor fluorophores in the PMT1 channel (514–526 nm) and for the acceptor fluorophores in the PMT2 channel (566–578 nm), in addition of brightfield imaging. Donor and acceptor z-stack images were analyzed pixel by pixel with a customized Matlab code to generate false color FRET ratio ($I_A/I_D$) images and FRET histograms for each image. Individual FRET z-stack images were stacked in ImageJ (NIH) and reconstructed in Volocity (PerkinElmer, Inc., MA) [26,29,30].

### 2.9. Immunostaining

ECMs were decellularized and fixed as previously described [21]. The ECMs were washed with 0.05% Triton X-100 (Thermo Scientific, IL) in PBS (PBS-X) for 5 min, then blocked for non-specific binding with PBS-X containing 1% SuperBlock (Thermo Scientific, IL). After washing twice with PBS-X, the samples were immunostained overnight at 4 °C for: Fn using either rabbit or mouse (when co-staining collagen I) antibodies (Sigma–Aldrich, MO), rabbit anti-mouse collagen I (Millipore, MA), mouse anti-talin (Millipore, MA), or rabbit phosphorylated focal adhesion kinase [pY379] (pFAK) (Invitrogen, CA). After overnight incubation, the samples were washed twice with PBS-X for 5min each, and incubated for 1 h at room temperature in a PBS-X/1% SuperBlock solution of the following formulations: DAPI (Life Technologies, NY) (1:5000), Alexa Fluor 568 Phalloidin (1:250), goat anti-rabbit Alexa Fluor 488 (1:100) or goat anti-mouse Alexa Fluor 488 (1:100), goat anti-mouse Alexa Fluor 647 (1:100) (All Alexa Fluorophores were obtained from Life Technologies, NY). After the secondary antibody incubation, samples were washed twice with PBS-X for 5 min, and kept in PBS for confocal microscopy imaging.

### 2.10. Analysis of matrix porosity and fiber diameter

Fn fiber diameters and matrix pore sizes were obtained from immunostained confocal microscope images and analyzed using ImageJ (NIH). To this end, 7 z-stack slices were orthogonally projected. Measurements were taken from random locations (including both

central and peripheral sample areas). Pore size was analyzed by measuring the average size of the empty spaces with fibers within the projection (as depicted in Fig. 3B).

### 2.11. VEGF secretion on cell-derived matrices

Preconditioned preadipocytes were seeded on Fn coated flat mica surfaces for 24 h as previously described. To compare between VEGF secretion and matrix sequestration, media was collected and cultures were decellularized and scraped, respectively. To understand how Fn matrix binding affects VEGF secretion, samples were decellularized, blocked for non-specific binding with PBS containing 1% bovine serum albumin for 20 min, sterilized with penicillin-streptomycin overnight, and washed twice with PBS. Untreated preadipocytes were trypsinized and suspended in serum free media with various integrin-blocking antibodies (3 μg/mL) on a shaker at 37 °C for 30 min. Cells were either left untreated, treated with only a rat anti-mouse integrin $\alpha_v$ blocker (CD51) (Millipore, MA), treated with only a rat anti-mouse $\beta_1$ blocker (CD29) (BD Biosciences, CA), or treated with both integrin blockers simultaneously. Cells were then allowed to attach in serum free media at 37 °C for 1 h, before switching to low serum media (1% FBS). After 3 h (total 4hr), the media were collected to quantify VEGF secretion with a Quantikine ELISA kit (R & D Systems, MN) and samples either extracted for DNA in Caron's buffer or fixed, immunostained, and imaged as previously described. VEGF secretion was normalized by μg of DNA for each corresponding sample and represented as a ratio relative to normalized VEGF secretion by untreated cells on control ECMs.

### 2.12. Statistics

Data were statistically analyzed in GraphPad Prism (GraphPad Software, Inc., CA). Student's t-tests or ANOVAs with Tukey's post-hoc tests were performed and statistical significance was determined at $p < 0.05$.

## 3. Results

### 3.1. Tumor-conditioned cells promote matrix stiffening through early altered Fn assembly

To evaluate if tumor cell-secreted factors alter ECM deposition by adipose stromal cells, a major cell type in the mammary microenvironment, we first used the Surface Forces Apparatus (SFA) to assess the overall rigidity of matrices deposited by tumor-associated and control 3T3-L1 preadipocytes (See Fig. 1). The SFA allows one to run compressive tests by determining the absolute distance *D* between two semi-reflecting smooth mica surfaces mounted on silica discs (Fig. 1A) using interferometric fringes patterns (Fig. 1B) while applying normal forces *F* via a double cantilever spring [22,23]. Briefly, tumor-associated and control 3T3-L1 cells were seeded onto the lower SFA mica disk in Fn-containing medium for 24 h (Fig. 1C) and later removed with decellularization buffer leaving behind a cell-free fibrillar ECM comprising Fn fibers (Fig. 1D, Fig. S1A). Compressive measurements were then performed in the quasi-static regime via the upper SFA (bare) mica disk and force–distance profiles were acquired (Fig. 1E). Data were further analyzed to extract elastic moduli using Johnson contact mechanics [24], in which the indentation of the matrix under compression $\delta$ is related to the normal force *F* by the following equation:

$$\frac{F}{R}=E\pi\frac{\delta^2}{D_0} \quad (1)$$

where $R$ is the radius of curvature of the discs, $D_0$ is the matrix thickness at rest, and $E$ the resulting Young modulus. Elastic moduli were calculated over a 25% strain range (Fig. 1F) and force normalized by radius of curvature ($F/R$) plotted as a function of thickness parameter $\delta^2/D_0$ was used as control for the fit quality (Fig. S1B). We found that the mean elastic moduli of unfixed/native tumor-associated ECM were significantly higher than those of control matrices ($E$ = 0.12 ± 0.04 vs. 0.07 ± 0.03 kPa, $p < 0.001$).

We have also tested the effect of *in situ* chemical fixation of the matrices (with neutral buffered formalin) on their rigidity and found it increased the stiffness of both tumor-associated and control matrices by 22% and 19%, respectively ($E$ = 0.14 ± 0.06 vs. 0.09 ± 0.05 kPa, $p < 0.002$) (Fig. S2), while the overall stiffening of tumor-associated matrices was maintained. These data indicate how essential it is to assess mechanical properties of cell-derived materials in their native state instead of using fixatives, which promotes extra stiffening (here by ~20%).

Since the ECM is a viscoelastic material, we next analyzed its creep response by applying instantaneous force and recording changes in ECM indentation depth (Δδ) over time (Fig. S3A). Our results indicate two time-dependent regimes that could be well fitted by a double exponential decay:

$$\Delta\delta(t)=A_1e^{\frac{-t}{\tau_1}}+A_2e^{\frac{-t}{\tau_2}} \quad (2)$$

where Δδ ($t$) is the matrix thickness decay, $\tau_1$ and $\tau_2$ are the fast and slow characteristic decay times, respectively, and $A_1$ and $A_2$ are the decay amplitudes used as fitting parameters. Tumor-conditioned matrices indicated longer decay times than control matrices in both the fast [$\tau_1$ = 125 ± 30 vs. 47 ± 25 s] and the slow [$\tau_2$ = 1048 ± 152 vs. 701 ± 107 s] regimes, suggesting a trend of overall slower responses of tumor-associated Fn matrices to external forces (Fig. S3B).

Collectively, these data indicate that, besides being stiffer, tumor-conditioned matrices may also be more viscous than their control counterpart, which is likely able to dysregulate mechanosignaling to surrounding cells. Although we could not find any previous report of tumor ECM viscoelasticity, our matrix creep data are in agreement with the enhanced viscosity detected in breast cancer [31] and prostate cancer [32] tissues. The relative poroelastic and viscoelastic contributions to the matrix characteristic decay times reported here are discussed later.

### 3.2. Early tumor-conditioned matrices comprise highly stretched and unfolded Fn fibers

We next combined FRET and confocal microscopy tomonitor the incorporation of FRET-labeled Fn into newly developed fibrils over 24 h, as previously described in Ref. [26] and calibrated in detail in Ref. [15] (Fig. 2). Our *in situ* FRET mapping shows that control cells (Fig. 2A) deposited high and medium FRET-Fn fibers (yellow and green pixels) indicative

of the coexistence of close-to-compact and extended Fn conformations. In contrast, tumor-associated cells (Fig. 2B) generated mostly stretched and unfolded Fn fibers, as indicated by low FRET fibrillar sections (blue pixels). Overall, tumor-associated matrices displayed both a more homogenous Fn population (narrower FRET histogram in Fig. 2C) and more stretched Fn fibers than control matrices (mean FRET intensity ratio = 0.35 ± 0.047 vs. 0.38 ± 0.05, $p < 0.0001$) (Fig. 2D). This trend is in agreement with previously published results [15]. Collectively, our data suggest that tumor-conditioned cells deposit Fn fibers with altered conformations that might alter Fn signaling either by exposing new binding sites to cells or by disrupting strain-sensitive binding motives such as the PHSRN synergy site and the RGD loop sequence responsible for $\alpha_5\beta_1$ integrin binding [33,34].

When testing the effect of Fn matrix chemical fixation on FRET, we found it increased the FRET ratio of control matrices (Fig. S4A) but had no effect on the FRET of tumor-conditioned (Fig. S4B) matrices, relative to unfixed conditions, denoting an overall strain relaxation and enhancing the differences between tumor-associated and control matrices (mean FRET intensity ratio = 0.35 ± 0.06 vs. 0.45 ± 0.05) (Fig. S4C, D).

### 3.3. Early tumor-conditioned Fn matrices are thicker, denser, and comprise thicker fibers

We next investigated the topology of the Fn matrices. We first used the SFA to assess ECM thickness (Fig. 3A) and show that tumor-conditioned cells generated a 37% thicker matrix than control cells ($D_0$ = 18.9 ± 1.7 vs. 13.7 ± 0.8 μm, $p < 0.03$). Next, z-projections of 3D reconstructed confocal image stacks (Fig. 3B) were used to quantify pore sizes and fiber diameters using ImageJ (NIH). We found that tumor-associated matrices were also denser, as indicated by smaller pores than in control matrices (73.3 ± 96.5 vs. 131.8 ± 179.8 $\mu m^2$) (Fig. 3C) and displayed Fn fibers with larger diameters ($Ø_{Tumor}$ = 1.10 ± 0.42 μm) than control matrices ($Ø_{Control}$ = 0.89 ± 0.31 μm) (Fig. 3D). Collectively, our data show that the topology of tumor-associated matrices is also altered: indeed, narrower pores and thicker Fn fibers likely contribute to enhanced matrix rigidity as well as altered cell binding and migration.

### 3.4. Early tumor-conditioned Fn matrices rapidly increase stromal cell proangiogenic factor secretion

To determine the relevance of our results in tumor angiogenesis, we next assessed the proangiogenic capability of fresh 3T3-L1s after their seeding onto the Fn matrices via quantification of vascular endothelial growth factor (VEGF) secretion after 4 h. This approach allowed us to ascertain cellular response to a matrix primarily consisting of Fn that has not yet been remodeled. Interestingly, our data indicate that tumor-conditioned Fn matrices inhibited adhesion (40%) relative to control (data not shown), while VEGF secretion was significantly enhanced in the tumor-conditioned ECMs compared to their control counterparts (34%, 1.338 ± 0.472 relative to control vs. 1 ± 0.318) (Fig. 4A). We attributed different levels of VEGF to altered secretion (1.326 ± 0.026 relative to control vs. 1 ± 0.105) rather than altered matrix sequestration after we analyzed Fn-matrix lysates indicating negligible amounts of Fn matrix-bound VEGF (approximately 9% of VEGF measured in the media) with no significant differences between tumor and control matrix conditions (0.086 ± 0.002 relative to control vs. 0.091 ± 0.018) (Fig. 4B). Because Fn

conformational changes were previously shown to modulate the binding specificity of integrins [35–39], we also examined altered integrin specificity as a potential mechanism of tumor-induced modified signaling. We initially tested whether introducing integrin blockers would alter VEGF secretion by exposing unconditioned 3T3-L1s to $\alpha_v$ blockers on control matrices and $\beta_1$ blockers on tumor matrices. We detected no significant difference in VEGF secretion on control and tumor matrices, respectively (Fig. 4C, +/− white bar and −/+ gray bar). We first tested the role of $\alpha_5\beta_1$ integrins in regulating VEGF secretion by exposing fresh cells to $\beta_1$ blockers prior to seeding. Our data indicate that blockade of $\beta_1$ dramatically increased VEGF secretion relative to the untreated-control condition (Fig. 4C, −/− and −/+ white bars) indicating that $\alpha_5\beta_1$-mediated interactions with control Fn, may contribute to low VEGF secretion levels by stromal cells. This effect was inhibited by simultaneous addition of an $\alpha_v$ function-blocking antibody (Fig. 4C, +/+ white bars), suggesting that $\alpha_v\beta_3$ may play a role in this process. We next tested the contribution of $\alpha_v\beta_3$ to increased VEGF secretion of cells interacting with tumor Fn. However, exposure of cells to $\alpha_v$ blockers prior to seeding led to a slight decrease in VEGF secretion (Fig. 4C, −/− and +/− gray bars), while concomitant blockade of both $\alpha_v$ and $\beta_1$ subunits further lowered VEGF secretion (Fig. 4C, +/+ gray bars), suggesting Fn-mediated complex integrin compensatory mechanisms [40]. Collectively, our data indicate that the presence of unfolded and stiff Fn fibers in tumor-conditioned matrices enhances 3T3-L1 secretion of VEGF by altering their use of $\alpha_v\beta_3$ over $\alpha_5\beta_1$ integrins. These results are discussed later and are in agreement with previous work by others showing a direct link between $\alpha_v\beta_3$ engagement and increased VEGF secretion [41].

Because cells respond to altered matrices by modulating their adhesive linkages, we further investigated cell adhesions by monitoring the recruitment of two focal adhesion proteins. Our data reveal differences in both talin and phosphorylated focal adhesion kinase (pFAK [pY397]) distribution among cells reseeded on control or tumor-associated matrices (Fig. S5). On control Fn, untreated cells recruited both talin and pFAK to develop fibrillar adhesions (insets: double arrows); instead, cells treated with $\beta_1$ blockers grew adhesive ECM clusters comprising mainly talin (Fig. S5, control). On tumor-conditioned Fn, untreated cells developed focal contacts comprising both talin and pFAK (insets: arrowheads) while cells treated with $\alpha_v$ blockers began developing fibrillar adhesion located mainly at the cell periphery (insets: double arrows) (Fig. S5, tumor). Interestingly, cells treated with both integrin blockers developed peripheral fibrillar adhesions on control Fn, and left behind ECM clusters on tumor-associated Fn.

Our findings are in agreement with previous work showing that focal contacts comprise primarily $\alpha_v\beta_3$ integrins whereas fibrillar (or mature) adhesions contain principally $\alpha_5\beta_1$ integrins [42]. These different adhesions are activated through different mechanisms: while $\alpha_5\beta_1$ integrins cluster and recruit adhesion proteins in a contractility-independent manner [43], $\alpha_v\beta_3$ integrins require cell contractility to develop nascent adhesions via talin [44], which regulates $\alpha_v\beta_3$ activation via a conformational change of $\beta_3$ reinforcing nascent focal contacts [45–47]. Our findings indicate that cells forced to utilize $\alpha_v\beta_3$ integrins on stiff and unfolded tumor-associated matrices recruit higher levels of talin to form large focal contacts, which may also modulate proangiogenic behavior.

## 4. Discussion

The experiments presented herein suggest that breast cancer cell-secreted factors deregulate early Fn matrix assembly by stromal cells. Increased levels of Fn had been previously detected in tumors [48], and plasma Fn is implicated in tumor growth [49]. Our findings additionally indicate that the mechanical and the structural/ conformational properties of Fn may be different in tumors vs. controls as matrices deposited by stromal cells in response to tumor-secreted factors exhibited increased overall stiffness, fiber stretching, and molecular unfolding. Moreover, these Fn alterations were linked to enhanced proangiogenic capability of the stromal cells with potential implications for tumor angiogenesis.

More specifically, tumor-conditioned matrices are mechanically different from control matrices as they exhibit increased stiffness. Our work also suggests that tumor-conditioned matrices have slower changes in indentation depth, indicative of both elastic and time-dependent (viscous) modifications. Furthermore, these matrices are structurally (and conformationally) altered across multiple length scales as they are overall thicker, denser, and composed of thicker fibers that comprise more unfolded Fn molecules. By combining the SFA with FRET mapping, our study provides a detailed picture of the early deposited Fn matrix from the matrix/cellular level to the molecular level. Our results are in accordance with work of previous investigators but also include new observations with direct implications on Fn-mediated tumor-stroma progression.

At the single fiber level, previous FRET work had shown that strain application to *manually-extruded* Fn fibers led to stiffening and unfolding (above 150% strain) in these fibers [26]. At the matrix level, another FRET study [15] estimated the average strain in *cell-derived* Fn fibers based on a FRET vs. strain calibration (performed on single *manually-extruded* fibers) and anticipated matrix stiffening although no direct measurement of matrix stiffness was performed. To our knowledge, this study reports the first quantitative and direct correlation between overall Fn matrix stiffness and topology at the matrix/cellular scale with Fn conformations at the molecular scale.

Our findings also underline how dramatic the effect of fixatives (commonly used in laboratories) can be on both the mechanical and structural properties of compliant (0.1 kPa range) and porous materials. Indeed, although the general trends of stiffening and unfolding were maintained for tumor-conditioned relative to control matrices, formalin increased rigidity and decreased strain (as indicated by a FRET increase), particularly in control Fn matrices where the random crosslinking of lysines likely resulted in the pinning of dangling/ relaxed Fn fibers in the network.

Our stiffness data indicate lower values for tumor-conditioned Fn matrices than for both macroscopic tumors *in vivo* [50] and single Fn fibers [27]. These difference can be attributed to (i) the higher porosity of cell-free Fn networks (with enhanced fluid transport) relative to the denser tumor tissue, (ii) the presence of both Fn and collagen in mature tumor tissues, and (iii) the different regime of deformations in individual fibers relative to ECM networks, where the deformation (here compression) is distributed over a mesh of disordered and connected fibers that respond collectively to stress by initially aligning/ordering along the

compressive surface before being further indented. Moreover our creep data indicate a trend of slower responses of tumor-conditioned matrices with respect to their control counterparts, with characteristic decay times of the order of $10^2$ and $10^3$ s for ($\tau_1$) and ($\tau_2$), comparable to the time of observation in our experiments. A simple calculation of the characteristic time for solvent molecules to be diffused through the Fn matrix, i.e., so-called poroelastic time $\tau_p$, assuming a typical radius of contact between SFA surfaces of 10 μm and a diffusion constant for cells and tissues of 10–100 $\mu m^2/s$ [51,52] leads to $\tau_p$ = 1–10 s, i.e., 10 to 100 times faster than the measured ($\tau_1$) and ($\tau_2$), Hence our results suggest that although poroelastic processes contribute to the biphasic system (Fn network + solvent) relaxation at shorter timescales, the longer decay times we report here are mainly due to viscoelasticity, i.e., conformational/structural changes in the Fn network rather than to solvent redistribution through the matrix pores.

Additionally, to obtain cell-derived Fn matrices, we used a well established protocol [21] comprising a mild detergent and multiple washing steps. Decellularizing matrices has previously been shown to (i) relax matrix networks by ~20% [53], and (ii) alter the ratio of DOC soluble (nascent) to DOC insoluble (crosslinked) Fn characterized herein [54], as DOC soluble Fn will have most likely been washed away. Although these effects should not alter our results, which report *relative* differences between control and tumor-conditioned decellularized matrices, future studies will be required to delineate the potential contribution of both relaxation and loss of fibrillar heterogeneity on these matrices, in particular by developing new (less invasive) decellularization protocols.

Matrix topology (denser network and thicker fibers) together with molecular unfolding of the initial Fn matrix may also influence indirectly the overall tumor-conditioned matrix mechanics. Additionally, on one hand, Fn unfolding has been shown to lead to the subsequent deposition of a more unfolded Fn matrix [29]. On the other hand, altered Fn characteristics might modulate tumor stiffness by altering the deposition of subsequent ECM components. For example, Fn fibers act as templates for the deposition of collagen [55]. In particular, the specific binding of collagen I α1 chain to the gelatin-binding domain of Fn (located on $FnI_6$, $FnII_{1–2}$, and Fn $III_{7–9}$) is necessary for the initial co-deposition of collagen [56]. Because the interaction of Fn with collagen is likely conformation dependent, the unfolded/highly strained Fn fibers initially generated by 3T3-L1s may dramatically affect collagen fibrillogenesis, either by disrupting the exposed binding site for collagen I or by exposing cryptic sites with enzymatic activity such as Fn type IV Col-ase, which is a matrix metalloprotease in the collagen binding domain of Fn capable of digesting collagen [57]. Consequently, Fn unfolding may also indirectly regulate the mechanosignaling of tumor-associated collagen I that ultimately contributes to tumorigenesis [11–13].

In this study, we also report that new (untreated) stromal cells seeded onto tumor-associated matrices exhibit decreased adhesion and enhanced VEGF secretion. Because tumor-conditioned Fn matrices exhibit topological, conformational, and mechanical alterations known to alter cell–matrix interactions, we hypothesized that Fn alterations might serve as a mechanosensor and “integrin switch”. Tumor-conditioned Fn ECMs were characterized to be dense matrices comprising thick fibers. Thicker fibers may alter ligand density, which in turn, would alter stable focal adhesion formation and downstream cellular behavior [58–61].

As increased ligand density might be another mechanism behind altered cell-Fn matrix interactions in tumors, future studies are needed to probe how antagonizing RGD binding sites could alleviate (in a dose-dependent manner) subsequent cell behavior in tumors. Our results indicate that the cells responsible for enhanced VEGF secretion detected on tumor-associated matrices (comprising mainly stretched/unfolded Fn fibers) tend to favor the use of $\alpha_v\beta_3$ over $\alpha_5\beta_1$ integrins to interact with Fn. This finding can be explained by differential engagement of either strain-sensitive (e.g., $\alpha_5\beta_1$) or strain-insensitive (e.g., $\alpha_v\beta_3$) integrins with the surrounding matrix. Indeed, the integrin binding $FnIII_9$–$III_{10}$ sequence of Fn is extremely sensitive to conformational changes resulting from enhanced tension exerted by cells. Earlier reports suggested that the distance between the "synergy" PHSRN site in $FnIII_9$ and the RGD site in $FnIII_{10}$ is critical for engagement and activation of integrin $\alpha_5\beta_1$ [62,63] but has little effect on engagement of integrin $\alpha_v\beta_3$. Therefore the "integrin switch" measured here on tumor-conditioned matrices may be in part explained by strain-induced increased spatial separation between $FnIII_9$ and $FnIII_{10}$ [35], which inhibits the binding of $\alpha_5\beta_1$ to both sites simultaneously [34] and forces cells to utilize more $\alpha_v\beta_3$ to compensate [36]. Our results are in agreement with previous work showing that higher engagement of $\alpha_v\beta_3$ increases VEGF secretion [38,41]. Moreover, we see that $\beta_1$ blockade of cells seeded on control (relaxed) Fn had a greater effect on VEGF secretion than $\alpha_v$ blockade of cells on tumor-conditioned (stretched) Fn. This functional difference may be attributed to VEGF receptor availability, as VEGF is immobilized to Fn through a $\alpha_5\beta_1$/VEGF-receptor [64]. This immobilization inhibits the accessibility of $\alpha_5\beta_1$, leading to VEGF release. Another explanation of the functional difference could be that $\alpha_5\beta_1$ has higher binding affinity (4 nM) to Fn [65] than $\alpha_v\beta_3$ (1.3 μM) [66]. Nevertheless, the measured increase in VEGF secretion may be further modulated by the physicochemical complexity of the tumor-conditioned ECM. This complexity not only entails differences in Fn stiffness and conformation (including different spatial distribution of ligands at the fiber surface), but also varied quantity and composition (e.g. proteoglycans), which can all regulate the observed integrin(s) switching effect. Though the difference in VEGF secretion is small, it is significant, and comparable to our previous studies in which similarly small differences in VEGF secretion on dense and mature ECM networks significantly affected endothelial cell behavior [38].

Collectively, our results contribute to an improved understanding of the role of early Fn matrix assembly in modulating proangiogenic factor secretion of breast tumor-conditioned stromal cells. Future experiments are needed to further clarify the role of Fn in a 3D tissue-like context. Our studies have been performed on cell-derived Fn-matrix coated mica surfaces, where both substrate rigidity and culture dimensionality can also regulate changes in cell behavior. In particular, the mica substrates used in our studies are stiffer than the tumor tissue, which may affect the mechanics and conformation of the deposited Fn matrix. Similarly, the formation of focal adhesions differs in 2D and 3D cell cultures [67] which also potentially modulates the properties of the Fn matrix. Future studies will (i) validate our integrin-modulated VEGF secretion findings in a physiologically relevant 3D matrix with controlled stiffness and topology, (ii) allow us to discriminate the roles of stiffness and conformation in regulating these processes [68], and (iii) lead to new insights that may improve current anti-VEGF therapies [69].

## 5. Conclusions

Our results indicate that, following exposure to breast cancer cell-secreted factors, adipose stromal cells initially deposit in the stroma, high amounts of stiff and unfolded Fn with altered topology, which deregulate the behavior of neighboring cells by modifying cell–matrix interactions (altered outside-in signaling). Our work also indicates that such tumor-induced Fn matrix deregulation activates integrin switches in surrounding cells ultimately enhancing VEGF secretion with potential functional consequences on tumor angiogenesis. These findings have important implications for our understanding of tumor growth, as they support the notion of Fn as a key initiator of mammary tumor angiogenesis. This work also enhances our knowledge of cell – Fn matrix mechanobiological interactions that may be exploited for other biomaterials-based applications, including advanced tissue engineering approaches.

## Supplementary Material

Refer to Web version on PubMed Central for supplementary material.

## Acknowledgments

Victoria Benson & Cory Brown for aid in image analysis and Juan Carlos Andresen & Shengling Hu for help in coding. Funding by NSF under award DMR-1352299 (to DG), NIH/NCI under award R01 CA185293 (to CF and DG) and U54 CA143876 (to CF), CONACYT under award 308671 (to RCAE), and the Cornell Center for Materials Research through Award Number (NSF DMR-1120296). Also, the Cornell University Biotechnology Resource Center (BRC) for data collected on the Zeiss LSM 710 Confocal (NIH 1S10RR025502-01).

## References

1. Spaeth EL, Dembinski JL, Sasser AK, Watson K, Klopp A, Hall B, et al. Mesenchymal stem cell transition to tumor-associated fibroblasts contributes to fibrovascular network expansion and tumor progression. PLoS One. 2009; 4:e4992. [PubMed: 19352430]
2. Mishra PJ, Mishra PJ, Humeniuk R, Medina DJ, Alexe G, Mesirov JP, et al. Carcinoma-associated fibroblast-like differentiation of human mesenchymal stem cells. Cancer Res. 2008; 68:4331–4339. [PubMed: 18519693]
3. Karnoub AE, Dash AB, Vo AP, Sullivan A, Brooks MW, Bell GW, et al. Mesenchymal stem cells within tumour stroma promote breast cancer metastasis. Nature. 2007; 449:557–563. [PubMed: 17914389]
4. Chandler EM, Seo BR, Californo JP, Andresen Eguiluz RC, Lee JS, Yoon CJ, et al. Implanted adipose progenitor cells as physicochemical regulators of breast cancer. Proc Natl Acad Sci U S A. 2012; 109:9786–9791. [PubMed: 22665775]
5. Butcher DT, Alliston T, Weaver VM. A tense situation: forcing tumour progression. Nat Rev Cancer. 2009; 9:108–122. [PubMed: 19165226]
6. Kumar S, Weaver VM. Mechanics, malignancy, and metastasis: the force journey of a tumor cell. Cancer Metastasis Rev. 2009; 28:113–127. [PubMed: 19153673]
7. Lu P, Weaver VM, Werb Z. The extracellular matrix: a dynamic niche in cancer progression. J Cell Biol. 2012; 196:395–406. [PubMed: 22351925]
8. Paszek MJ, Zahir N, Johnson KR, Lakins JN, Rozenberg GI, Gefen A, et al. Tensional homeostasis and the malignant phenotype. Cancer Cell. 2005; 8:241–254. [PubMed: 16169468]
9. Fischbach C, Kong HJ, Hsiong SX, Evangelista MB, Yuen W, Mooney DJ. Cancer cell angiogenic capability is regulated by 3D culture and integrin engagement. Proc Natl Acad Sci U S A. 2009; 106:399–404. [PubMed: 19126683]

10. Calvo F, Ege N, Grande-Garcia A, Hooper S, Jenkins RP, Chaudhry SI, et al. Mechanotransduction and YAP-dependent matrix remodelling is required for the generation and maintenance of cancer-associated fibroblasts. Nat Cell Biol. 2013; 15:637–646. [PubMed: 23708000]
11. Levental KR, Yu H, Kass L, Lakins JN, Egeblad M, Erler JT, et al. Matrix cross-linking forces tumor progression by enhancing integrin signaling. Cell. 2009; 139:891–906. [PubMed: 19931152]
12. Provenzano PP, Eliceiri KW, Campbell JM, Inman DR, White JG, Keely PJ. Collagen reorganization at the tumor-stromal interface facilitates local invasion. BMC Med. 2006; 4:38. [PubMed: 17190588]
13. Provenzano PP, Inman DR, Eliceiri KW, Knittel JG, Yan L, Rueden CT, et al. Collagen density promotes mammary tumor initiation and progression. BMC Med. 2008; 6:11. [PubMed: 18442412]
14. Mammoto A, Connor KM, Mammoto T, Yung CW, Huh D, Aderman CM, et al. A mechanosensitive transcriptional mechanism that controls angiogenesis. Nature. 2009; 457:1103–1108. [PubMed: 19242469]
15. Chandler EM, Saunders MP, Yoon CJ, Gourdon D, Fischbach C. Adipose progenitor cells increase fibronectin matrix strain and unfolding in breast tumors. Phys Biol. 2011; 8:015008. [PubMed: 21301062]
16. Midwood KS, Williams LV, Schwarzbauer JE. Tissue repair and the dynamics of the extracellular matrix. Int J Biochem Cell Biol. 2004; 36:1031–1037. [PubMed: 15094118]
17. Sottile J, Hocking DC. Fibronectin polymerization regulates the composition and stability of extracellular matrix fibrils and cell-matrix adhesions. Mol Biol Cell. 2002; 13:3546–3559. [PubMed: 12388756]
18. Anderson JM. Biological responses to materials. Annu Rev Mater Res. 2001; 31:81–110.
19. Zhang Y, Lu H, Dazin P, Kapila Y. Squamous cell carcinoma cell aggregates escape suspension-induced, p53-mediated anoikis: fibronectin and integrin alphav mediate survival signals through focal adhesion kinase. J Biol Chem. 2004; 279:48342–48349. [PubMed: 15331608]
20. Curran CS, Keely PJ. Matrix biology. Matrix Biol. 2013; 32:95–105. [PubMed: 23262216]
21. Castelló-Cros R, Cukierman E. Stromagenesis during tumorigenesis: characterization of tumor-associated fibroblasts and stroma-derived 3D matrices. Methods Mol Biol. 2009; 522:275–305. [PubMed: 19247611]
22. Israelachvili JN. Thin film studies using multiple-beam interferometry. J Colloid Interface Sci. 1973; 44:259–272.
23. Israelachvili JN, McGuiggan PM. Adhesion and short-range forces between surfaces. Part I: new apparatus for surface force measurements. J Mater Res. 1990; 5:2223–2231.
24. Johnson, KL. Contact mechanics. Cambridge University Press; 1985.
25. Baneyx G, Baugh L, Vogel V. Coexisting conformations of fibronectin in cell culture imaged using fluorescence resonance energy transfer. Proc Natl Acad Sci U S A. 2001; 98:14464–14468. [PubMed: 11717404]
26. Smith ML, Gourdon D, Little WC, Kubow KE, Eguiluz RA, Luna-Morris S, et al. Force-induced unfolding of fibronectin in the extracellular matrix of living cells. Plos Biol. 2007; 5:e268. [PubMed: 17914904]
27. Klotzsch E, Smith ML, Kubow KE, Muntwyler S, Little WC, Beyeler F, et al. Fibronectin forms the most extensible biological fibers displaying switchable force-exposed cryptic binding sites. Proc Natl Acad Sci U S A. 2009; 106:18267–18272. [PubMed: 19826086]
28. Little WC, Schwartlander R, Smith ML, Gourdon D, Vogel V. Stretched extracellular matrix proteins turn fouling and are functionally rescued by the Chaperones albumin and casein. Nano Lett. 2009; 9:4158–4167. [PubMed: 19743815]
29. Antia M, Baneyx G, Kubow KE, Vogel V. Fibronectin in aging extracellular matrix fibrils is progressively unfolded by cells and elicits an enhanced rigidity response. Faraday Discuss. 2008; 139:229. [PubMed: 19048998]
30. Antia M, Islas LD, Boness DA, Baneyx G, Vogel V. Single molecule fluorescence studies of surface-adsorbed fibronectin. Biomaterials. 2006; 27:679–690. [PubMed: 16095684]

31. Sinkus R, Tanter M, Catheline S, Lorenzen J, Kuhl C, Sondermann E, et al. Imaging anisotropic and viscous properties of breast tissue by magnetic resonance-elastography. Magn Reson Med. 2005; 53:372–387. [PubMed: 15678538]
32. Zhang M, Nigwekar P, Castaneda B, Hoyt K, Joseph JV, di Sant'Agnese A, et al. Quantitative characterization of viscoelastic properties of human prostate correlated with histology. Ultrasound Med Biol. 2008; 34:1033–1042. [PubMed: 18258350]
33. Ruoslahti E. Fibronectin and its receptors. Annu Rev Biochem. 1988; 57:375–413. [PubMed: 2972252]
34. Pierschbacher MD, Ruoslahti E. Cell attachment activity of fibronectin can be duplicated by small synthetic fragments of the molecule. Nature. 1984; 309:30–33. [PubMed: 6325925]
35. Krammer A, Craig D, Thomas WE, Schulten K, Vogel V. A structural model for force regulated integrin binding to fibronectin's RGD-synergy site. Matrix Biol. 2002; 21:139–147. [PubMed: 11852230]
36. Petrie TA, Capadona JR, Reyes CD, García AJ. Integrin specificity and enhanced cellular activities associated with surfaces presenting a recombinant fibronectin fragment compared to RGD supports. Biomaterials. 2006; 27:5459–5470. [PubMed: 16846640]
37. Friedland JC, Lee MH, Boettiger D. Mechanically activated integrin switch controls alpha5beta1 function. Science. 2009; 323:642–644. [PubMed: 19179533]
38. Wan AMD, Chandler EM, Madhavan M, Infanger DW, Ober CK, Gourdon D, et al. Fibronectin conformation regulates the proangiogenic capability of tumor-associated adipogenic stromal cells. Biochim Biophys Acta. 2013; 1830:4314–4320. [PubMed: 23567798]
39. Seong J, Tajik A, Sun J, Guan J-L, Humphries MJ, Craig SE, et al. Distinct biophysical mechanisms of focal adhesion kinase mechanoactivation by different extracellular matrix proteins. Proc Natl Acad Sci U S A. 2013; 110:19372–19377. [PubMed: 24222685]
40. Hynes RO. A reevaluation of integrins as regulators of angiogenesis. Nat Med. 2002; 8:918–921. [PubMed: 12205444]
41. De S, Razorenova O, McCabe NP, O'Toole T, Qin J, Byzova TV. VEGF-integrin interplay controls tumor growth and vascularization. Proc Natl Acad Sci U S A. 2005; 102:7589–7594. [PubMed: 15897451]
42. Zamir E, Geiger B. Molecular complexity and dynamics of cell-matrix adhesions. J Cell Biol. 2001; 114:3583–3590.
43. Schiller HB, Hermann M-R, Polleux J, Vignaud T, Zanivan S, Friedel CC, et al. β1- and αv-class integrins cooperate to regulate myosin II during rigidity sensing of fibronectin-based microenvironments. Nat Cell Biol. 2013; 15:625–636. [PubMed: 23708002]
44. Jiang G, Giannone G, Critchley DR, Fukumoto E, Sheetz MP. Two-piconewton slip bond between fibronectin and the cytoskeleton depends on talin. Nature. 2003; 424:334–337. [PubMed: 12867986]
45. Wegener KL, Partridge AW, Han J, Pickford AR, Liddington RC, Ginsberg MH, et al. Structural basis of integrin activation by talin. Cell. 2007; 128:171–182. [PubMed: 17218263]
46. Critchley DR. Biochemical and structural properties of the integrin-associated cytoskeletal protein talin. Annu Rev Biophysics. 2009; 38:235–254.
47. Roca-Cusachs P, del Rio A, Puklin-Faucher E, Gauthier NC, Biais N, Sheetz MP. Integrin-dependent force transmission to the extracellular matrix by α-actinin triggers adhesion maturation. Proc Natl Acad Sci U S A. 2013:1–18.
48. Stenman S, Vaheri A. Fibronectin in human solid tumors. Int J Cancer. 1981; 27:427–435. [PubMed: 7024140]
49. Au von A, Vasel M, Kraft S, Sens C, Hackl N, Marx A, et al. Circulating fibronectin controls tumor growth. Neoplasia. 2013; 15:925–938. [PubMed: 23908593]
50. Samani A, Zubovits J, Plewes D. Elastic moduli of normal and pathological human breast tissues: an inversion-technique-based investigation of 169 samples. Phys Med Biol. 2007; 52:1565–1576. [PubMed: 17327649]
51. Moeendarbary E, Valon L, Fritzsche M, Harris AR, Moulding DA, Thrasher AJ, et al. The cytoplasm of living cells behaves as a poroelastic material. Nat Mater. 2013; 12:253–261. [PubMed: 23291707]

52. Rosenbluth MJ, Crow A, Shaevitz JW, Fletcher DA. Slow stress propagation in adherent cells. Biophysical J. 2008; 95:6052–6059.
53. Kubow KE, Klotzsch E, Smith ML, Gourdon D, Little WC, Vogel V. Crosslinking of cell-derived 3D scaffolds up-regulates the stretching and unfolding of new extracellular matrix assembled by reseeded cells. Integr Biol. 2009; 1:635–648.
54. McKeown-Longo PJ, Mosher DF. Binding of plasma fibronectin to cell layers of human skin fibroblasts. J Cell Biol. 1983; 97:466–472. [PubMed: 6309861]
55. Sottile J, Shi F, Rublyevska I, Chiang HY, Lust J, Chandler J. Fibronectin-dependent collagen I deposition modulates the cell response to fibronectin. AJP Cell Physiol. 2007; 293:C1934–C1946.
56. McDonald JA, Kelley DG, Broekelmann TJ. Role of fibronectin in collagen deposition: Fab' to the gelatin-binding domain of fibronectin inhibits both fibronectin and collagen organization in fibroblast extracellular matrix. J Cell Biol. 1982; 92:485–492. [PubMed: 7061591]
57. Schnepel J, Tschesche H. The proteolytic activity of the recombinant cryptic human fibronectin type IV collagenase from E. coli expression. J Protein Chem. 2000; 19:685–692. [PubMed: 11307953]
58. Cavalcanti-Adam EA, Volberg T, Micoulet A, Kessler H, Geiger B, Spatz JP. Cell spreading and focal adhesion dynamics are regulated by spacing of integrin ligands. Biophysj. 2007; 92:2964–2974.
59. Arnold M, Schwieder M, Blümmel J, Cavalcanti-Adam EA, López-Garcia M, Kessler H, et al. Cell interactions with hierarchically structured nano-patterned adhesive surfaces. Soft Matter. 2009; 5:72–77. [PubMed: 21686049]
60. Geiger B, Spatz JP, Bershadsky AD. Environmental sensing through focal adhesions. Nat Rev Mol Cell Biol. 2009; 10:21–33. [PubMed: 19197329]
61. Bradshaw MJ, Smith ML. Multiscale relationships between fibronectin structure and functional properties. Acta Biomater. 2013; 10:1524–1531. [PubMed: 23978411]
62. Obara M, Kang MS, Yamada KM. Site-directed mutagenesis of the cell-binding domain of human fibronectin: separable, synergistic sites mediate adhesive function. Cell. 1988; 53:649–657. [PubMed: 3286012]
63. Aota S, Nagai T, Yamada KM. Characterization of regions of fibronectin besides the arginine-glycine-aspartic acid sequence required for adhesive function of the cell-binding domain using site-directed mutagenesis. J Biol Chem. 1991; 266:15938–15943. [PubMed: 1874740]
64. Wijelath ES, Murray J, Rahman S, Patel Y, Ishida A, Strand K, et al. Novel vascular endothelial growth factor binding domains of fibronectin enhance vascular endothelial growth factor biological activity. Circulation Res. 2002; 91:25–31. [PubMed: 12114318]
65. Takagi J, Strokovich K, Springer TA, Walz T. Structure of integrin alpha5beta1 in complex with fibronectin. Embo J. 2003; 22:4607–4615. [PubMed: 12970173]
66. Liu Y, Pan Y, Xu Y. Binding investigation of integrin alphavbeta3 with its inhibitors by SPR technology and molecular docking simulation. J Biomol Screen. 2010; 15:131–137. [PubMed: 20086207]
67. Fraley SI, Feng Y, Krishnamurthy R, Kim D-H, Celedon A, Longmore GD, et al. A distinctive role for focal adhesion proteins in three-dimensional cell motility. Nat Cell Biol. 2010; 12:598–604. [PubMed: 20473295]
68. Janmey PA, Weitz DA. Dealing with mechanics: mechanisms of force transduction in cells. Trends Biochem Sci. 2004; 29:364–370. [PubMed: 15236744]
69. Cao Y, Langer R. Optimizing the delivery of cancer drugs that block angiogenesis. Sci Transl Med. 2010; 2:15ps3.

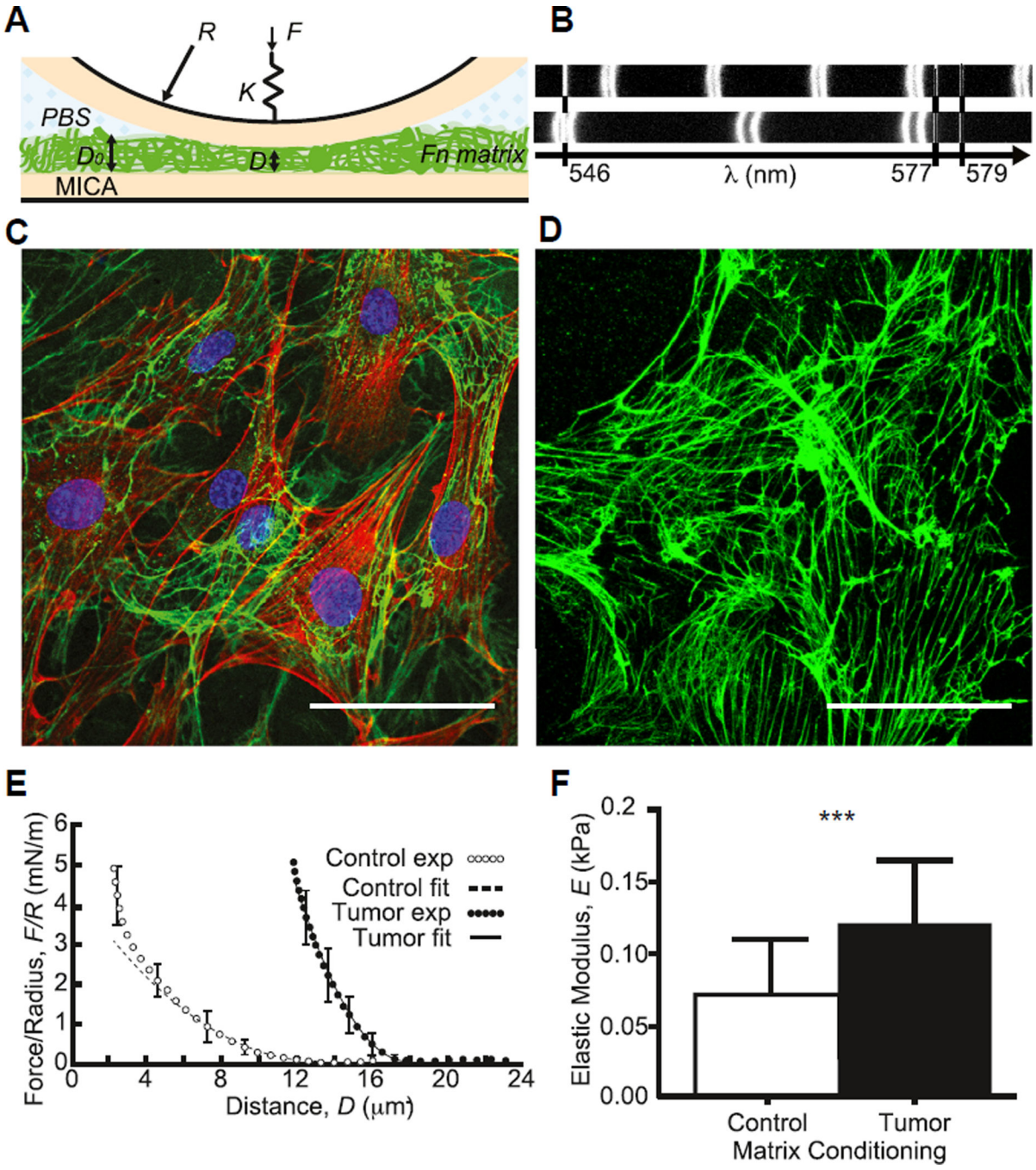


**Fig. 1.**

Tumor-associated Fn matrices are stiffer. (A) Schematics of the Surface Forces Apparatus (SFA) mica surfaces and setup used for mechanical characterization of the matrices at 37 °C. (B) Interference fringes measured with the SFA when shining white light through the confining surfaces at large (uncompressed matrix) and small (compressed matrix) separations. (C) Immunostaining of tumor-conditioned stromal cells embedded in their ECM after 24 h of culture onto SFA mica surfaces (green, Fn; red, F-actin; and blue, nuclei). (D) Same as (C) after decellularization (cell extraction) showing the Fn matrix left behind. Scale

bars = 50 μm. (E) To determine Fn matrix stiffness, compressive force–distance profiles were acquired in quasi-static conditions in control (○) and tumor-associated (●) conditions and fitted using a Hertzian model. (F) Mean tumor-associated matrix elastic moduli (n = 18) were ~60% higher than those of control matrices (n = 20). (For interpretation of the references to color in this figure legend, the reader is referred to the web version of this article.)

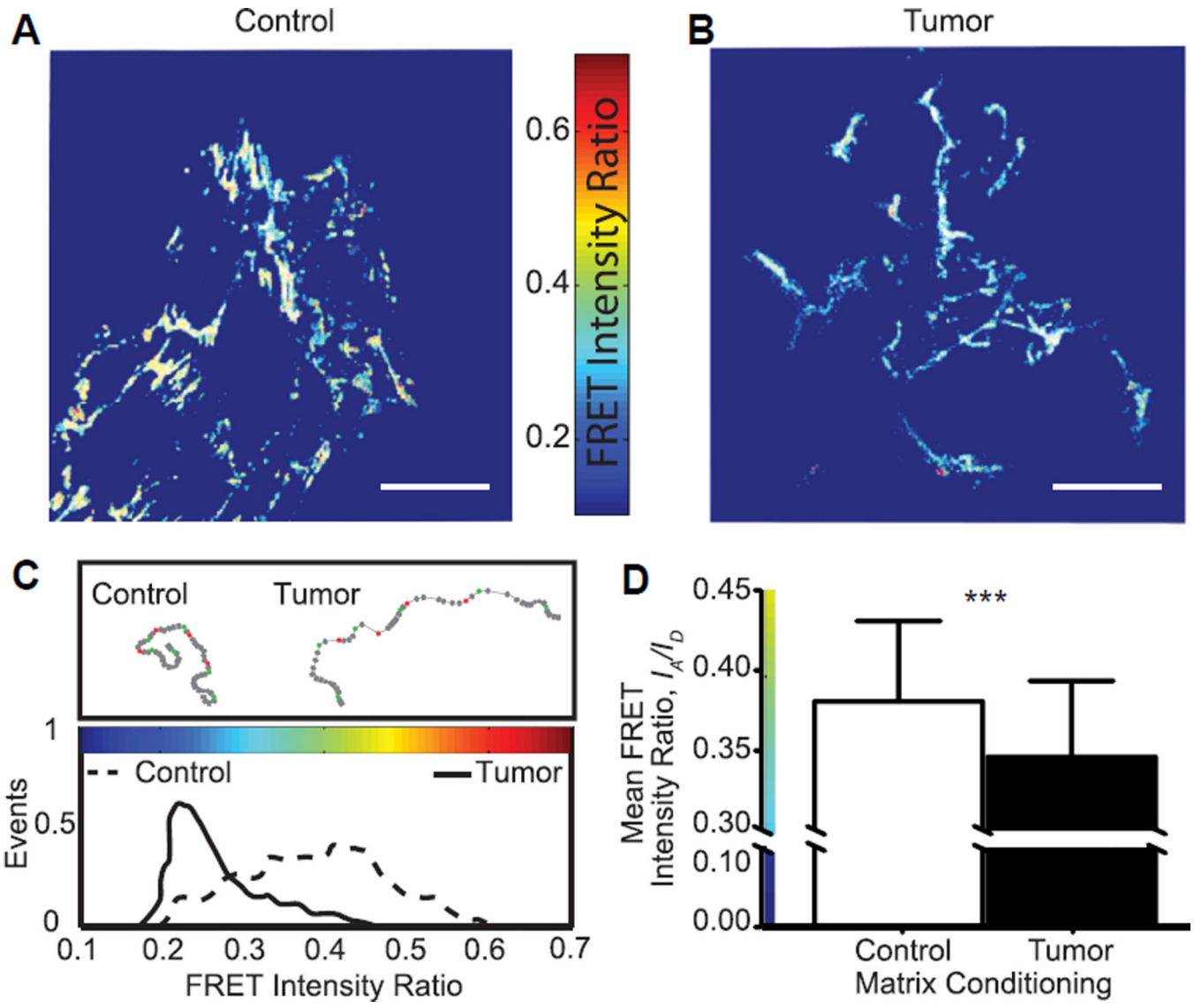


**Fig. 2.**

Tumor-associated Fn matrices are more unfolded. (A, B) FRET-Fn maps showed lower FRET intensity ratios, $I_A/I_D$, in tumor matrices (blue Fn fibers) than in their control counterpart (green/yellow Fn fibers). Scale bars = 50 μm. (C) Corresponding FRET intensity ratio histograms confirmed that tumor-associated Fn matrices comprised mainly stretched/unfolded Fn fibers (low FRET, narrow distribution) while control matrices contained a broader population of Fn conformations (higher FRET, larger distribution). (D) Mean FRET intensity ratios, $I_A/I_D$, of tumor-associated Fn matrices (n = 171) were lower than that of control matrices (n = 245), indicating that tumor conditions increased unfolding by ~10% with respect to control. Mean ± SD. (For interpretation of the references to color in this figure legend, the reader is referred to the web version of this article.)

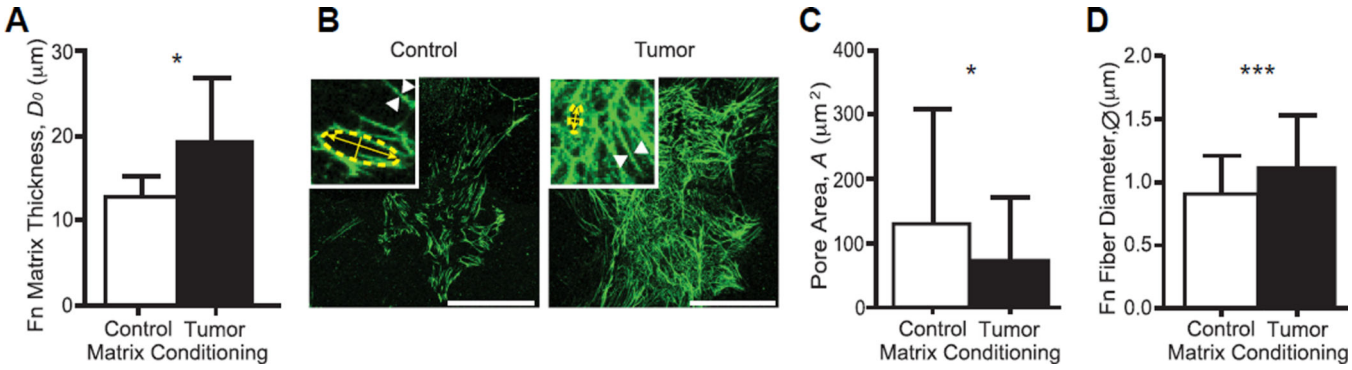


**Fig. 3.**

Tumor-associated Fn matrices are thicker, denser, and comprised thicker fibers. (A) Tumor-associated Fn matrices (n = 21) measured by the SFA were thicker than control matrices (n = 17). (B) Z-projections of immunostained control and tumor-associated Fn matrices. Scale bars = 50 μm. Insets: 300% zooms used to determine the pore size and fiber diameter shown in panels (C) and (D), respectively. (C) Pores measured within tumor-associated Fn matrices (n = 72) were significantly smaller than those measured within control matrices (n = 72) ($p < 0.0001$). (D) Tumor-associated Fn fibers (n = 120) possessed larger diameters than those of control Fn fibers (n = 120) ($p < 0.05$). Mean ± SD.

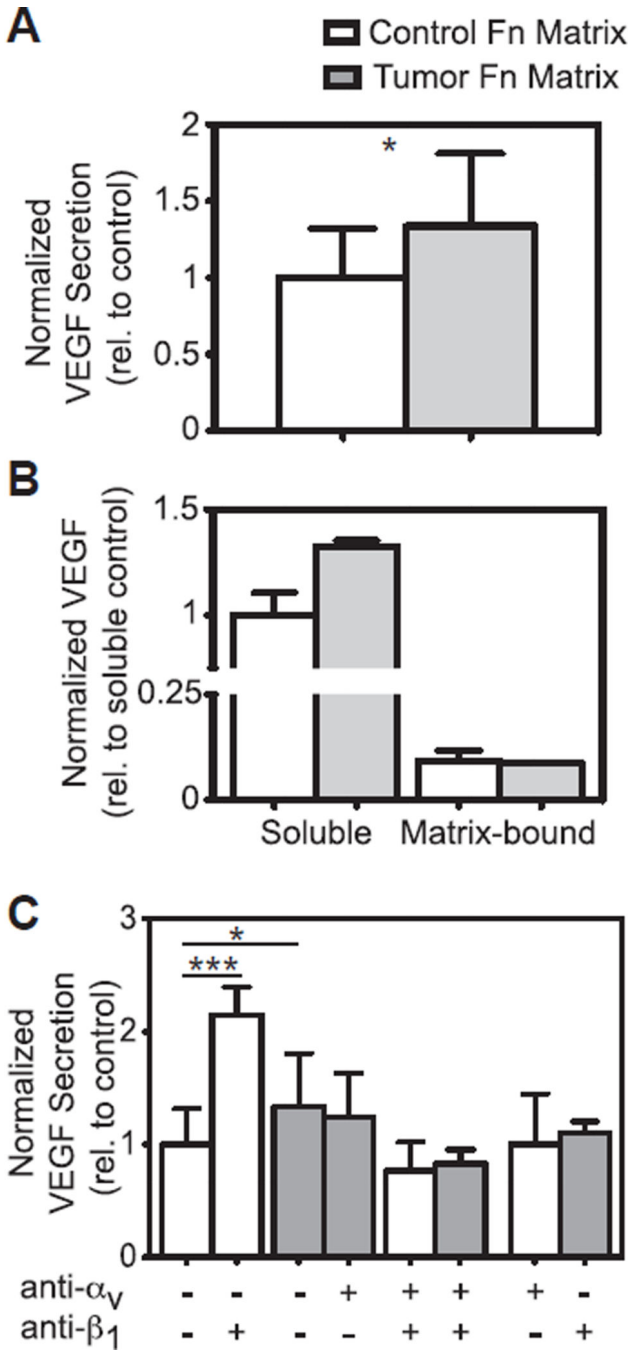


**Fig. 4.**

Cells adhere to tumor-associated Fn preferentially through $\alpha_v$ integrins with associated increased VEGF secretion. (A) After 4 h, new (untreated) cells secreted significantly higher levels of VEGF when seeded onto tumor-associated Fn (1.338 ± 0.472 relative to control, n = 13) than those seeded onto control Fn (1 ± 0.318, n = 14) ($p < 0.05$). (B) There were differences in VEGF secretion (1.326 ± 0.026 relative to control vs. 1 ± 0.105) but not in matrix sequestration from the same samples after 24 h cultures (0.086 ± 0.002 relative to control vs. 0.091 ± 0.018). n = 2/group. (C) After 4 h, cells treated with $\beta_1$-integrin blockers

and seeded onto control ECMs secreted significantly higher levels of VEGF than untreated cells (2.153 ± 0.246 relative to control, n = 6 vs. 1 ± 0.318, n = 14) ($p < 0.0001$). When cells treated with $\alpha_v$-integrin blockers were seeded onto control ECMs, no change in VEGF secretion was detected compared to untreated cells (1 ± 0.449, n = 4). Cells treated with $\alpha_v$-integrin blockers and seeded onto tumor ECMs secreted slightly lower levels of VEGF than untreated cells (1.242 ± 0.392 relative to control, n = 6 vs. 1.338 ± 0.472, n = 13). For cells treated with $\beta_1$-integrin blockers on tumor ECMs, there was an insignificant decrease in VEGF secretion compared to untreated cells (1.098 ± 0.108, n = 4). As a control, cells treated with both integrin blockers secreted lower levels of VEGF on both control (0.767 ± 0.253, n = 6) and tumor ECMs (0.828 ± 0.126, n = 6). Mean ± SD.